ADVANCED FUNCTIONAL MATERIALS
www.afm-journal.de

A Vertically-Stacked Optoelectronic Sensor for Localized Hemodynamics Monitoring

Taeyeon Lee, Jieun Jung, Hyeongoh Park, Dongwuk Jung, Doyune Kim, Changeui Hong, Seungbeom Kang, Hyunsoo Kim, Tae Kim, and Jongho Lee**

Optoelectronic sensors are widely used as they monitor important biosignals in real-time, many times in non-invasive ways by making use of the degree of light absorption through live tissues. In many of the applications, the optoelectronic sensors in a small form factor with attachable or insertable forms enable understanding the critically important biological states and mechanisms, including localized activities in very complex biological environments, such as in the brain. In this report, an optoelectronic sensor is presented, built by vertically integrating two different micro light emitting diodes (microLEDs) next to a photodetector with a predetermined interoptode distance in attachable or insertable forms. Both of the optical simulations and experimental results validate the designs and capabilities of the approach, by demonstrating the sensors on a human finger, around femoral vessels in a mouse model, and in mouse brains to monitor optogenetically-induced localized hemodynamics.

1. Introduction

Biological signals provide crucial clues for understanding the states and mechanisms of biological systems including humans.[1] Among many types of sensing approaches, optoelectronic sensors usually composed with paired light sources and photodetectors have become widely used for real-time monitoring of biological signals in ways of photoplethysmography (PPG),[2,3] near-infrared spectroscopy (NIRS),[4,5] and pulse oximeter.[6–9] The optoelectronic sensors are advantageous as they can measure critically important physiological signals such as blood flow and oxygen saturation in a wearable form during daily activities or in an implantable form for medical procedures and studies around the heart following open-heart surgery,[10] the grafted organs to monitor postoperative progress,[5,11] or the brain to monitor oxygen saturation in response to inhaled oxygen supply.[12]

While these methods may be enough in some applications, capability of monitoring localized tissue hemodynamics at a very specific point would help a deeper understanding complex activities in live bodies, such as brain circuit connectivity, by detecting local neural activity when stimulated at a very confined region, for example, by optogenetic stimulation in the complex brain environments. Currently, hemodynamics in the brain is monitored by a craniotomy optical imaging spectroscopy,[13–15] a laser doppler flowmeter probe,[15–17] a bundle of optical fibers[18,19] or a functional magnetic resonance imaging (fMRI) scan.[13,16] These methods enable only observing the surface activities[20] or require bulky instrumentations, including lasers or dedicated facilities.

Here, we present a localized hemodynamics sensor in a way of vertically stacking two different micro LEDs to have more common paths of light to a photodetector in a more compact space, enabling for more localized monitoring of hemodynamics in a specific target region. Designs of the different interoptode distances (from LEDs to PD) also allow measurements in different depths of interest from the sensor depending on applications. We demonstrate the feasibility of the approach by applying the sensors to monitor hemodynamics including blood flowing and oxygen saturation, with hypoxic challenge tests and optogenetic stimulations in attachable and insertable forms for a human subject and mouse models, highlighting its potential for a wide range of biomedical applications, including neurovascular coupling studies.

T. Lee, H. Park[+], D. Jung[++], D. Kim, C. Hong, S. Kang, H. Kim, J. Lee
School of Mechanical Engineering
Gwangju Institute of Science and Technology (GIST)
123 Cheomdangwagi-ro, Buk-gu, Gwangju 61005, Republic of Korea
E-mail: jong@gist.ac.kr

J. Jung, T. Kim
Department of Biomedical Science and Engineering
Gwangju Institute of Science and Technology (GIST)
123 Cheomdangwagi-ro, Buk-gu, Gwangju 61005, Republic of Korea
E-mail: tae-kim@gist.ac.kr

The ORCID identification number(s) for the author(s) of this article can be found under https://doi.org/10.1002/adfm.202504564

[+]Present address: Department of Electrical and Computer Engineering, Inter-University Semiconductor Research Center, Seoul National University, Seoul 08826, Republic of Korea

[++]Present address: Department of Mechatronics Engineering, Chonnam National University, 50 Daehak-ro, Yeosu 59626, Republic of Korea

DOI: 10.1002/adfm.202504564

2. Results and Discussion

2.1. Vertically-Stacked Multicolor Micro-LEDs for Hemodynamics Monitoring

Hemodynamics monitoring such as tissue oxygen saturation (StO_2) rely on different ratios of light-tissue interactions such as absorption through biological tissues interested in, depending on wavelengths of light, as illustrated in **Figure** 1a. Vertically-stacked (V-stacked) ultrathin μLEDs with different bandgaps enables multicolor μLEDs that can serve as a light source from one common point in a relative thin and small form factor. Figure 1b shows the design of the hemodynamics sensor by integrating heterogeneous multicolor μLEDs (blue: GaN on top, red: AlGaInP at the bottom) aligned vertically and a photodetector (PD: GaAs) laterally at a predetermined interoptode distance. The interoptode distance can be determined by considering various factors such as the wavelength of the LEDs, the transmittance and absorption coefficient of the tissue being observed, and the depth of the region of interest.[4,11]

Figure 1c shows the fabricated hemodynamics sensor by integrating the blue LED (bandgap: ≈2.70 eV, size: 250 × 300 μm^2, thickness: 5.0 μm), the red LED (bandgap: ≈1.85 eV, size: 250 × 300 μm^2, thickness: 4.1 μm) and PD (bandgap: ≈1.42 eV, size: 500 × 500 μm^2, thickness: 4.2 μm) on a flexible substrate (Polyimide, PI, 25 μm), after being fabricated from the source wafers and released by an epitaxial lift-off process. More details of the fabrication process are provided in the Experimental Section. The V-stacked multicolor LEDs look as one device from the top-view optical image (Figure 1c). The interoptode distance is 750 μm. The size (device region: 1.5 × 0.5 mm^2, red dashed box) and overall thickness (≈60 μm) of the hemodynamic sensor are comparable with a grain of rice (Figure 1d) and a single human hair (Figure 1e), respectively. More details are in Figure S1 (Supporting Information).

The multicolor LEDs can emit different colors depending on the relative ratios of injected current to the top (blue) and bottom (red) LED as shown in Figure 1f. When an electrical current is applied only to the top GaN LED, the color of the LED is blue (inset image in Figure 1g, corresponding to the peak wavelength (≈460 nm) as shown with the spectral irradiance in Figure 1g. Although an electrical current is applied to the hidden bottom LED (AlGaInP), the red light is visible from the top (inset image in Figure 1h) as the top GaN LED has a higher bandgap energy (2.7 eV) than the energy (1.85 eV) of the photons emitted from the bottom AlGaInP LED. The peak wavelength measured is ≈670 nm as shown in Figure 1h. Turning on both of the top and bottom LEDs emits violet with two peak wavelengths as in Figure 1i. The external quantum efficiency (EQE) of the GaAs photodetector is also shown in Figure 1i, indicating that the PD can detect both of the blue (≈460 nm) and red (≈670 nm) light. With the single PD, temporal control of the LEDs was used to avoid crosstalk by alternately turning on and off the blue and red LEDs as confirmed in Figure S2 (Supporting Information). The fabricated V-stacked hemodynamic sensors can be used in various applications to monitor biosignals on a finger, near blood vessel, and brain in attachable or insertable forms as in Figure S3 (Supporting Information).

2.2. Optical, Electrical and Mechanical Characteristics of the Hemodynamic Sensor

The V-stacked hemodynamic sensor occupies less physical dimension but provides more common paths of back-scattered light as shown with three different designs (V-stacked, laterally-placed, and oppositely-placed) in **Figure** 2a–c. The side view (Figure 2d) and top view (Figure 2e) of the photon paths visualized by optical simulations (Ansys Zemax OpticStudio), indicate that the V-stacked design (first in Figure 2d,e) has more common paths of the red and blue light, compare to the laterally-placed (second) and oppositely-placed (third). The total counts of the voxels (10 × 10 × 10 μm^3) occupied by the red or blue light paths separately are similar (350 000–390 000) for all three designs but the V-stacked design has much more voxels (122 165) of the common paths than those of the laterally-designed (98 634) and the oppositely-placed (53 903) as shown in Figure 2f. More details about the optical simulation are described in the Experimental Section and Figure S4 (Supporting Information).

The current–voltage (I–V) characteristics of the red and blue LEDs in the flexible hemodynamic sensor are comparable with those fabricated on the wafer as shown in Figure 2g. The measured photocurrents generated in the PD (Figure 2h) at the interoptode distance (750 μm) by backscattered light through isolated porcine skin tissues from the red and blue LEDs are 339 and 25.5 nA at zero bias, respectively. It should be noted that Effects by ambient light(36.45 μA, under one sun illumination (AM1.5G, 100 mW cm^{-2}, XES-70S1, SAN-EI Electric Ltd.)) was significantly reduced (≈1 V → 0.137 V) as the PD was facing to skin tissues. In addition, the flexible sensor was covered with a black cloth which blocks remaining ambient light almost completely (0.137 V → 0.019 V) during the experiments in addition to using a transimpedance amplifier and noise filters whenever required. More details are in Figures S5 and S6 (Supporting Information) and Experimental Section.

Since the inorganic μLEDs and PD are integrated onto a PI film, the fabricated V-stacked hemodynamic sensor is mechanically flexible enough to be bent at a radius of curvature of 5 mm, as in Figure 2i. The finite element analysis (FEA, ABAQUS) in Figure 2j indicates that the mechanical strain to the semiconductors is within ±0.15% (maximum tensile strain: 0.15% on the photodetector, maximum compressive strain: −0.11% on the red LED) at the bending radius of 5 mm, which is comparable to that of a human finger. We also conducted additional finite element simulations to analyze strain levels under various bending radii (3 mm to 9.43 mm) as summarized in Figure S7 (Supporting Information). The electrical performance (FF: fill factor, J_{sc}: short circuit current density, $V_{forward}$: forward voltage at 1.0 mA) remains stable without significant degradation when repetitive mechanical flexibility tests were conducted up to 10 000 bending cycles at a frequency of 0.1 Hz as in Figure 2k. Because the custom-setup is based on the low-speed, high-precision motorized stage (2 μm), the tests were conducted at a relatively slow rate but with high degree of bending (radius: 5 mm). More details of the performance are in Figure S8 (Supporting Information).

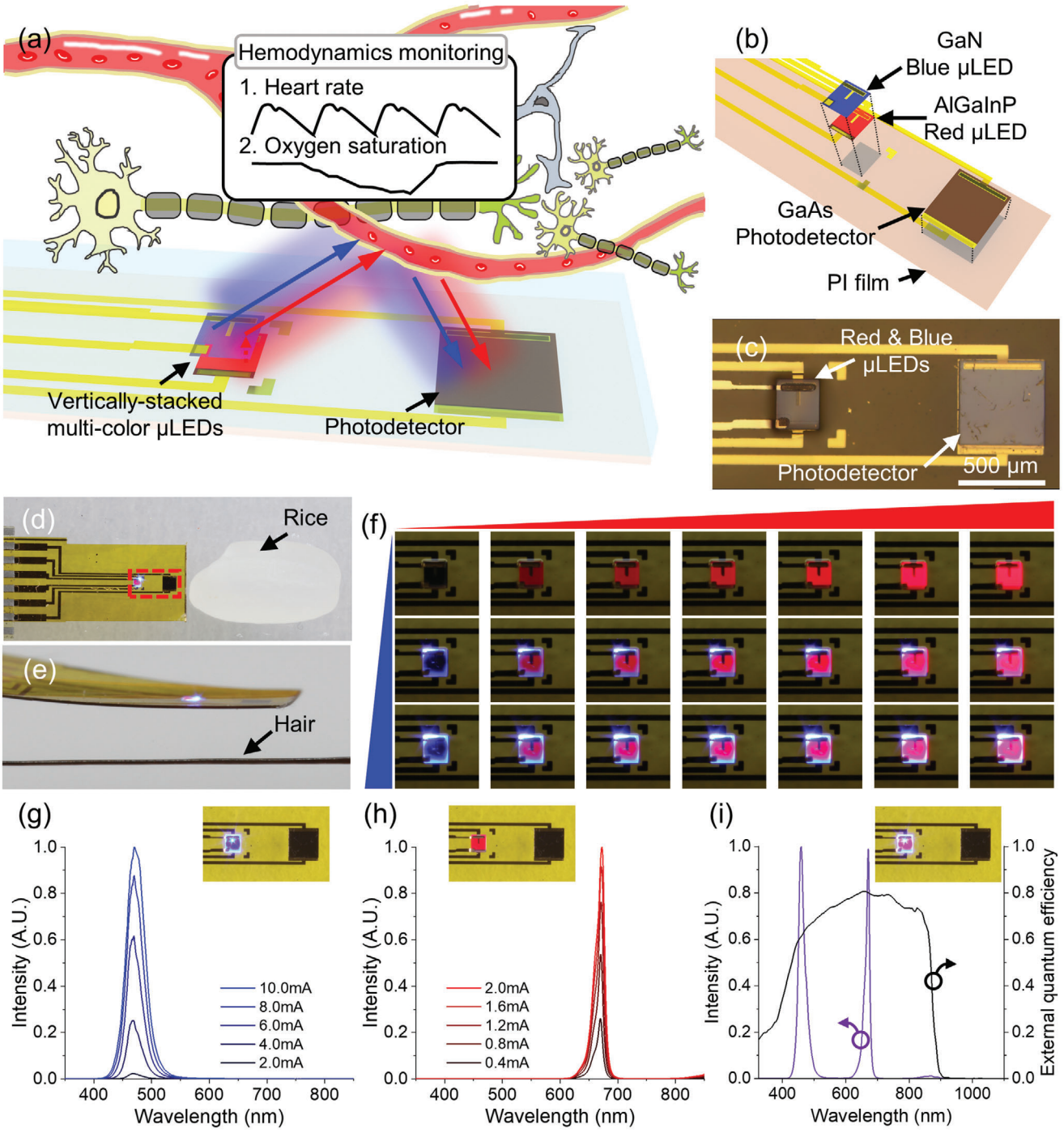

Figure 1. Vertically-stacked (V-stacked) multicolor micro-LEDs with a photodetector (PD) for hemodynamics monitoring. a) Schematic illustration of the vertically-stacked multicolor (blue on the top and red at the bottom) LEDs and a photodetector for optical hemodynamic monitoring. Both blue light (≈460 nm) and red light (≈670 nm) which passes through the blue LED are transmitted through the biological tissues, and detected by the neighboring photodetector. b) Integration of the red LED (AlGaInP, bandgap: ≈1.85 eV) and the blue LED (GaN, bandgap: ≈2.70 eV) aligned vertically, next to the photodetector (GaAs) on the flexible substrate (PI film, thickness: 25 μm). c) Optical microscope image of the fabricated hemodynamic monitoring sensor with two LEDs (red LED thickness: 4.1 μm, blue LED thickness: 5.0 μm, and both LEDs size: 250 × 300 μm^2), and photodetector (thickness: 4.2 μm, size: 500 × 500 μm^2). The two LEDs are vertically aligned at the exactly same location, appearing as a single LED. d,e) Optical images of the sensor (size: ≈1.5 × 0.5 mm^2, thickness: ≈60 μm) to compare the dimension with a grain of rice and human hair. f) Variable colors from the vertically-stacked LEDs by modulating the input voltage to the LEDs independently. Spectral characteristics of the multicolor LEDs when a current is applied g) only to the GaN LED (blue), h) only to the AlGaInP LED (red), and i) to both the LEDs (purple). The color (inset images) is adjustable depending on the applied currents to the LEDs. External quantum efficiency (EQE) of the fabricated GaAs photodetector is ≈0.6 and 0.8 at the peak wavelengths (red: 670 nm, blue: 460 nm).

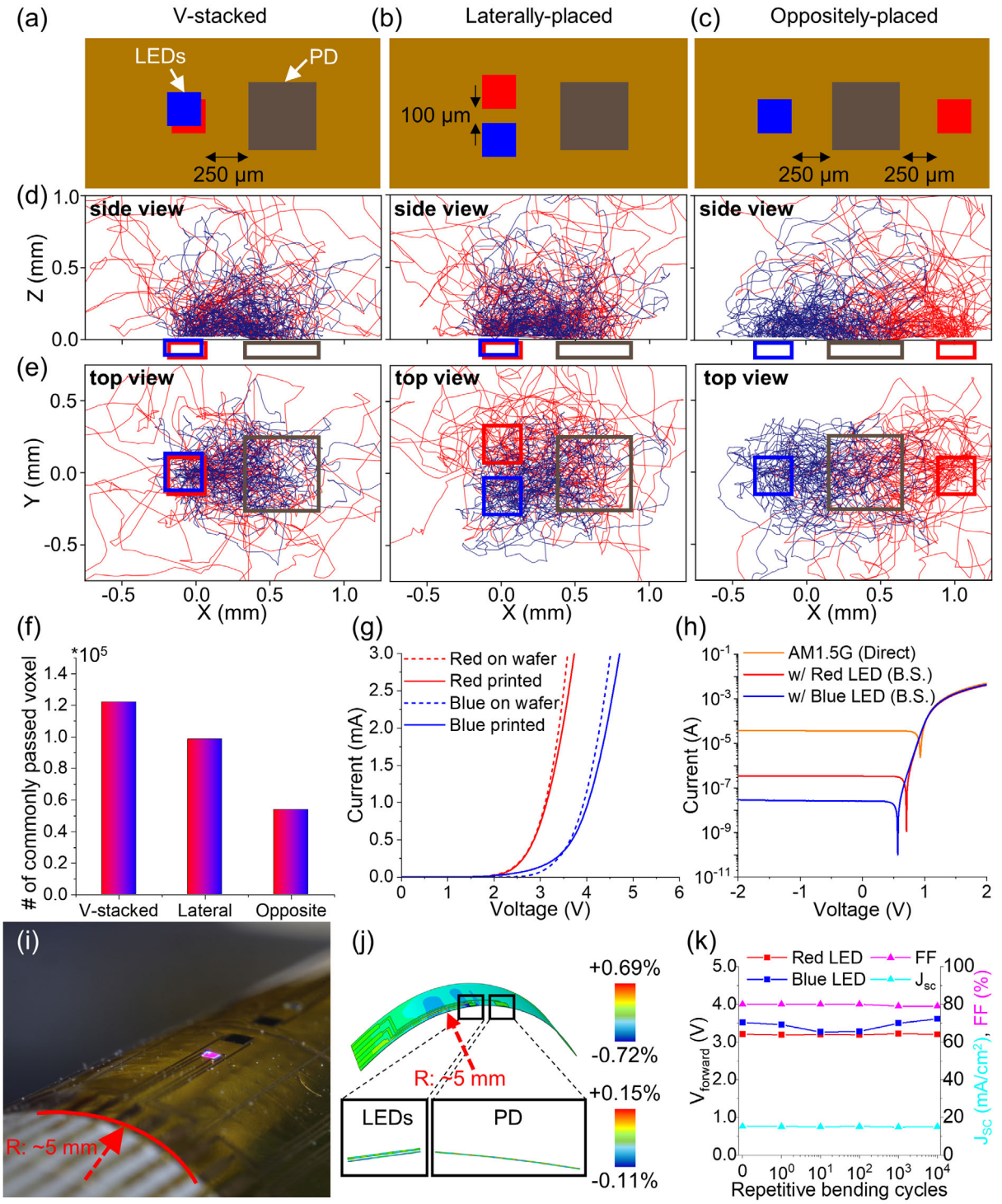

Figure 2. Optical, electrical, and mechanical characteristics of the V-stacked hemodynamic sensor. Schematic illustrations of the sensor design with a) vertically-stacked, b) laterally-placed, and c) oppositely-placed LEDs alongside a photodetector. d) Side, and e) top view of the optical simulation results of V-stacked (first), laterally-placed (second), and oppositely-placed (third) design. The positions of photodetector (brown box), red (red box), and blue (blue box) LEDs are also indicated. f) The number of voxels commonly passed by red and blue photons in each design. The V-stacked design shows 24% more than the laterally-placed, and 127% more than the oppositely-placed design. g) Current–voltage (*I–V*) characteristics of the red and blue LEDs before and after transfer-printing from each wafer to PI film. h) Current–voltage (*I–V*) characteristics of the photodetector under direct illumination with a solar simulator (power: 100 mW cm^{-2}, one sun, AM1.5G), and back-scattered (B.S.) light from the red and blue LEDs through porcine skin. i) Optical image of the V-stacked hemodynamic sensor (total thickness: ≈60 μm) bent with a radius of curvature of 5 mm. j) Mechanical strain distribution of the hemodynamic sensor including LEDs and PD with a bending radius of 5 mm. k) Forward voltage ($V_{forward}$) of the red and blue LEDs, and short circuit current density (J_{SC}) and fill factor (FF) of the photodetector under repetitive mechanical bending cycles (frequency: 0.1 Hz) at a radius of 5 mm.

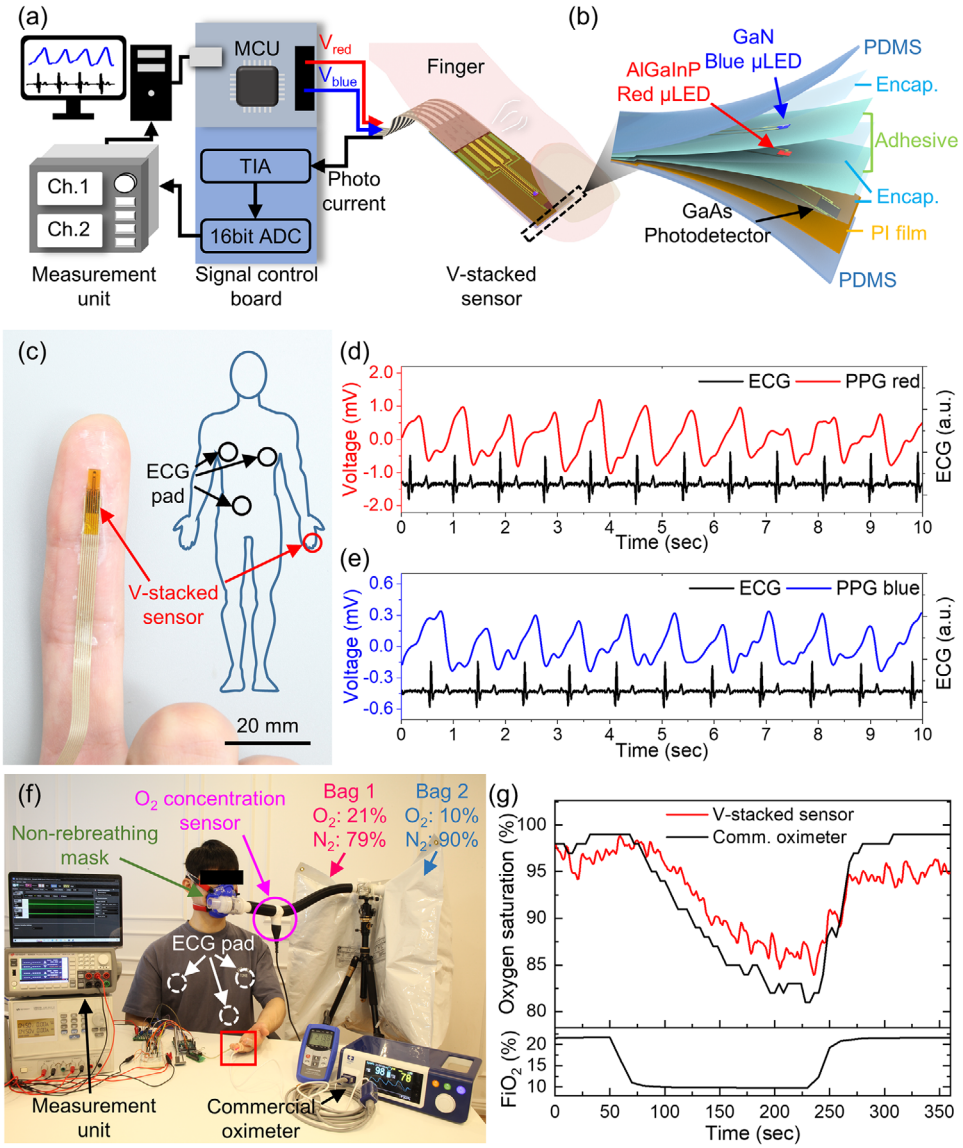

Figure 3. Attachable hemodynamic monitoring for a human subject. a) Custom setup for the real-time monitoring from the V-stacked sensor. b) Schematic illustration of the V-stacked hemodynamic sensor encapsulated with the soft elastomer (PDMS, 30:1, Sylgard 184) to be attachable to skin. c) Optical image of the fabricated V-stacked sensor attached on a human finger. Commercial electrocardiography (ECG) pads are attached for comparison (Inset illustration). d,e) Measured photoplethysmography (PPG) signals from the V-stacked sensor with illumination (d) from the red LED and (e) from the blue LED, respectively. The heart rates from the V-stacked sensor match exactly with those from the ECG sensor. f) Experimental set-up for measuring oxygen saturation during a hypoxic challenge test in a human subject. Oxygen concentration is controlled by mixing inhaling gas from the bags with different air compositions (Bag 1: O_2 21%/ N_2 79%, Bag 2: O_2 10% / N_2 90%). The oxygen concentration (Fraction of inspired oxygen, FiO_2) of the mixed inhaling gas is monitored with a commercial O_2 concentration sensor (magenta circle). The oxygen saturation in blood measured from the attached V-stacked sensor is compared with the measurements from a commercial oxygen saturation sensor attached to the neighboring finger (in red box). g) Measured oxygen saturation from hypoxic challenge test in a human subject. Oxygen saturation from the V-stacked sensor (red line) drops as FiO_2 is reduced from 21% to 10% at 50 s (lower plot), matching with the measurement from the commercial sensor (black line).

2.3. Attachable Hemodynamics Monitoring for a Human Subject

The V-stacked sensor can be used to monitor hemodynamics such as photoplethysmography (PPG) and tissue oxygen saturation in a non-invasive attachable form for a human subject. **Figure** 3a is a schematic illustration of the custom setup for real-time monitoring of hemodynamic signals with the V-stacked sensor. The red and blue light from the multicolor LEDs are alternatively modulated by the programmable microcontroller unit (MCU, Arduino Mega 2560). The back-scattered light is captured by the photodetector that generates photocurrent depending on red or blue light intensity through tissues. The photocurrent is amplified by the transimpedance amplifier (TIA) and then converted to digital signals by the analog-to-digital converter (ADC, ADS1115, Texas Instruments) for real-time monitoring or recording in the measurement unit.

The skin attachable V-stacked sensor in Figure 3b was designed to have an interoptode distance of 750 μm because the interoptode distance provides the mean penetration depths of blue (0.61 mm) and red (0.80 mm), which is deeper than the epidermis thickness (0.2–0.4 mm) of a human index finger.[21] In cases with variations in tissue characteristics such as fat layer thickness, the sensors with different interoptode distances (250–1750 μm) can be chosen. For example, for an individual with a higher obesity level (thicker subcutaneous fat layers), the V-stacked sensor with a longer interoptode distance could be used to enable monitoring of vascular signals at deeper region. Optical simulations and analysis indicate that, although increased interoptode distance enables deeper penetration, it also reduces the signal intensity due to longer optical paths. In addition, the light passing through multiple tissue layers, is subject to increased scattering and absorption, which may further lower the signal-to-noise ratio. More details described in Figures S9 and S10 (Supporting Information). The whole sensor was encapsulated with a sticky elastomer (PDMS 30:1) to make intimate contact to a finger. When necessary, additional tape can be applied to ensure contact to minimize unwanted noise caused by the air gap between the sensor and the finger.

Figure 3c shows the fabricated V-stacked sensor attached to a human index finger to measure PPG signals. Commercial electrocardiography (ECG) sensor (EVAL-AD8233, Analog Devices) pads are also attached to the human subject for heart rate signal comparison. The measured PPG signals based on the red or blue LED are shown in Figure 3d,e, respectively. The measurements with the attachable V-stacked sensor represent the standard PPG signals with the same pulse rates measured with the commercial ECG sensor (66 to 72 bpm.).

The V-stacked multicolor LEDs in the attachable form enable measurements of tissue oxygen saturation in a human subject. Figure 3f shows the experimental setup for a hypoxic challenge test based on the standard protocol (ISO80601-2-61).[22] The oxygen concentration of the air the subject breath in can be controlled with a valve from the breathing bags (bag1: normal mixture (O_2 21%/ N_2 79%), bag 2: hypoxic mixture (O_2 10%/ N_2 90%)). The fraction of inspired oxygen (FiO_2) is monitored in the tube connect to the face mask and the non-rebreathing valve is attached to prevent exhaled air from coming back to the mask. The tissue oxygen saturation measured with the V-stacked hemodynamics sensor attached on the index finger was compared with the result by a commercial sensor (bedside SpO_2 monitoring system, Nellcor) mounted on the adjacent middle finger. More details about the experimental setup are in Experimental Section.

The measured tissue oxygen saturation changes with the V-stacked sensor for the human subject are shown in Figure 3g (upper plot), conducted during the hypoxic challenge test by controlling the fraction of inspired oxygen (FiO_2) down from 21% to 10% at 60 s and maintaining until 240 s (lower plot). The tissue oxygen saturation change can be calculated based modified Beer-Lambert law, with measurements in the PD by alternatively turning on and off red and blue light from multicolor LEDs as the absorption coefficients of oxyhemoglobin (HbO) and deoxyhemoglobin (HbR) are different at different wavelengths (460, 670 nm). The measured tissue oxygen saturation (red line) decreases gradually from an initial value of 98% to 85% in the hypoxia, then recovered close to normal (≈95%) when the hypoxia is finished, comparable to the result with a commercial sensor (black line). The higher fluctuation in the V-stacked sensor is attributed to subject's movement during measurement. While commercial sensors display oxygen content with reduced fluctuation by sensing with intimate contact by clipping onto peripheral sites, and by updating the measured data every 2 to 4 s, our sensor was designed in an attachable form to continuously monitor the signal with the moving average filter (window size: 1 s). The fluctuation in the signal can be reduced by attaching the sensor more intimately with an aid of additional tapes or other methods. In addition, the fluctuation can be further reduced by adjusting the window size of the moving average filter depending on time scales to be measured.

2.4. Insertable Hemodynamic Monitoring for an Animal Model

The V-stacked multi-LEDs sensor can be used to measure hemodynamics in a needle-like insertable form by integrating on a rigid shuttle, followed by multilayer encapsulation to avoid damage from biofluids, as illustrated in **Figure 4a**. More details of fabrication process are in Experimental section. Figure 4b shows the fabricated insertable hemodynamic sensor (width: 1 mm) with a shorter interoptode distance (ρ = 250 μm). The shorter interoptode distance allows more localized measurements as shown with the optical simulations in Figure S9 (Supporting Information). The multilayer encapsulation (SU-8: ≈80 μm, PDMS: ≈50 μm and parylene: ≈10 μm) was enough to prevent damage from biofluids as confirmed with a soaking test. The electrical characteristics did not show significant degradation even after the insertable sensor being immersed in PBS (phosphate buffered saline) solution for 2 weeks as in Figure 4c. More details of the performance are in Figure S11 (Supporting Information).

The V-stacked sensor can be inserted subcutaneously through a small incision near the femoral vessel region of a mouse model (SKH1-Hr^{Hr}, Figure 4d, Detailed descriptions are in Figure S12, Supporting Information) to monitor PPG signals as shown in Figure 4e (with red light) and 4f (with blue light). The PPG-based heart rates (150 to 162 bpm.) of the mouse match well with the simultaneous measurements by using a commercial ECG sensor.

Tissue oxygen saturation can be also measured with the insertable V-stacked sensor. Hypoxic challenge tests were conducted with the mouse model (SKH1-Hr^{Hr}) in the custom-built hypoxia chamber with controllable supply lines for medical-grade oxygen and nitrogen in Figure 4g. Hemodynamic signals were recorded with the V-stacked sensor inserted around the femoral region of the mouse model while controlling and monitoring fraction of inspired oxygen (FiO_2) with a commercial oxygen concentration sensor next to the mouse model in the chamber. As FiO_2 was reduced down to 10% ≈100 s (lower plot in Figure 4h), the oxygen saturation in the femoral region of the mouse decreased down to 60% and started to recover gradually when FiO_2 came back to ≈22.5%, indicating that the V-stacked sensor enough to monitor the hemodynamics in the insertable form.

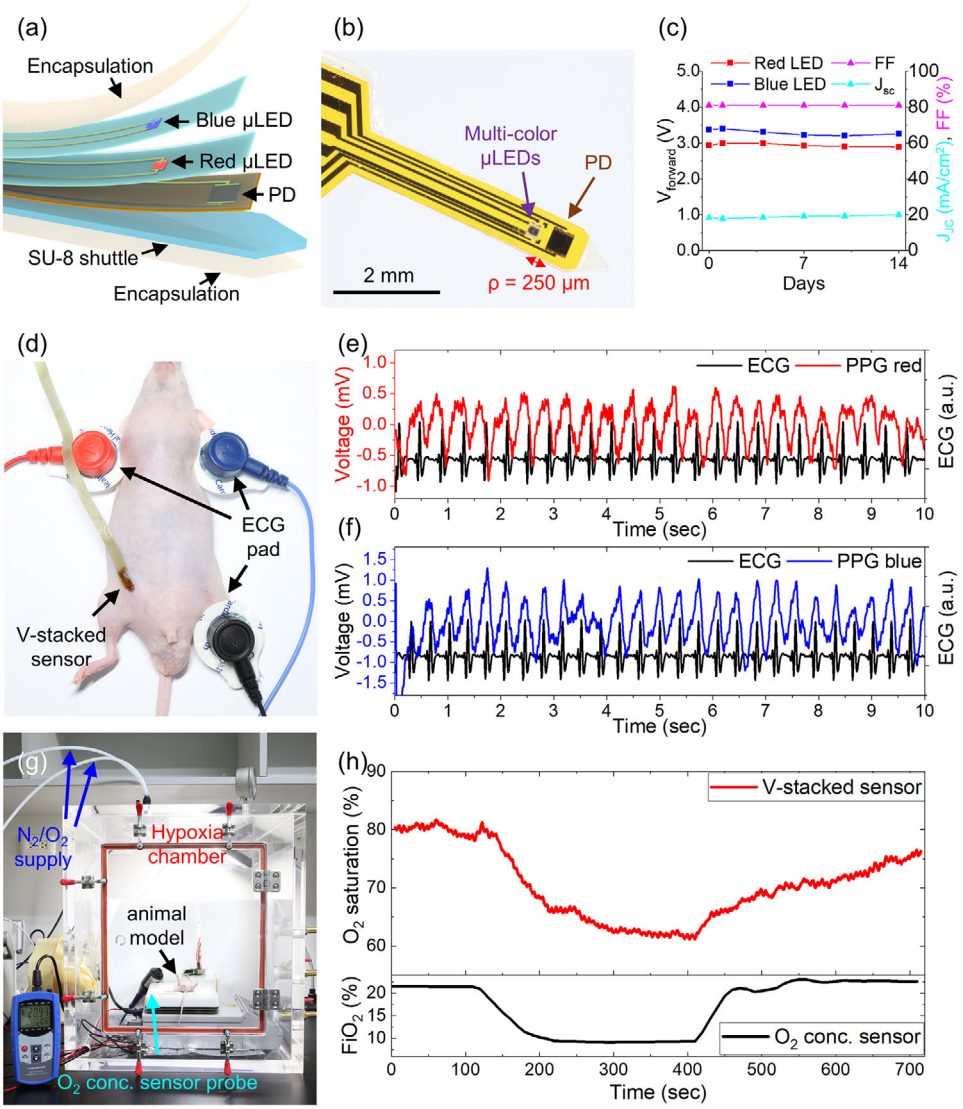

Figure 4. Insertable hemodynamic monitoring for an animal model. a) Design of the insertable V-stacked hemodynamic sensor integrated on the rigid polymer shuttle (SU-8 2075). The sensor is encapsulated with multiple polymer layers (SU-8, PDMS, and parylene). b) Optical image of the insertable V-stacked hemodynamic sensors fabricated with the shorter interoptode distance (ρ = 250 μm). c) Electrical characteristics of the sensors ($V_{forward}$: forward voltage of the LEDs, J_{SC}: short circuit current density of the PD, FF: fill factor of the PD) for two weeks soaking in PBS (phosphate buffered saline). d) Experimental setup for heart rate monitoring with the V-stacked sensor inserted around the femoral vessels. Commercial ECG pads are attached for comparison. e,f) Measured PPG results from the V-stacked sensor with (e) the red LED on or (f) the blue LED on. The heart rates from the PPG signals match with those from the ECG sensor. (150–160 bpm.). g) Custom-built hypoxic challenge chamber to measure the tissue oxygen saturation of the animal model depending on fraction of inspired oxygen (FiO_2) which is monitored with a commercial O_2 concentration sensor placed near the mouse head. h) Measurement results with the insertable V-stack hemodynamic sensor for the animal model in the hypoxic challenge chamber. The measured oxygen saturation (StO_2, red line) drops following the reduced inhaled oxygen concentration (FiO_2, black line) from 21% to 10% ≈100 s. The oxygen saturation recovers as the inhaled oxygen concentration increases back to 22.5%.

2.5. Optogenetically-Induced Localized Neurovascular Hemodynamics Monitoring

The small form factor of the V-stacked sensor enables monitoring of localized neurovascular hemodynamics in a brain as illustrated in **Figure** 5a. The V-stacked sensor inserted in a particular brain region of interest monitors optogenetically-induced localized activities near specific neurons such as parvalbumin (PV) neurons when the neurons expressing channelrhodopsin-2 (ChR2) are locally stimulated with a particular wavelength of light through an optical fiber. In this work, we targeted to stimulate and monitor PV neurons in the somatosensory barrel field of mouse models. The mouse models (PV-Cre mouse) were prepared by injecting adeno-associated virus (AAV) for expressing blue light activated cation channel, ChR2. More details about the procedure are in Experimental Section. In case of monitoring hemodynamic signals in deep brain regions such as the hippocampus, the experimental setup should be carefully designed by taking into account

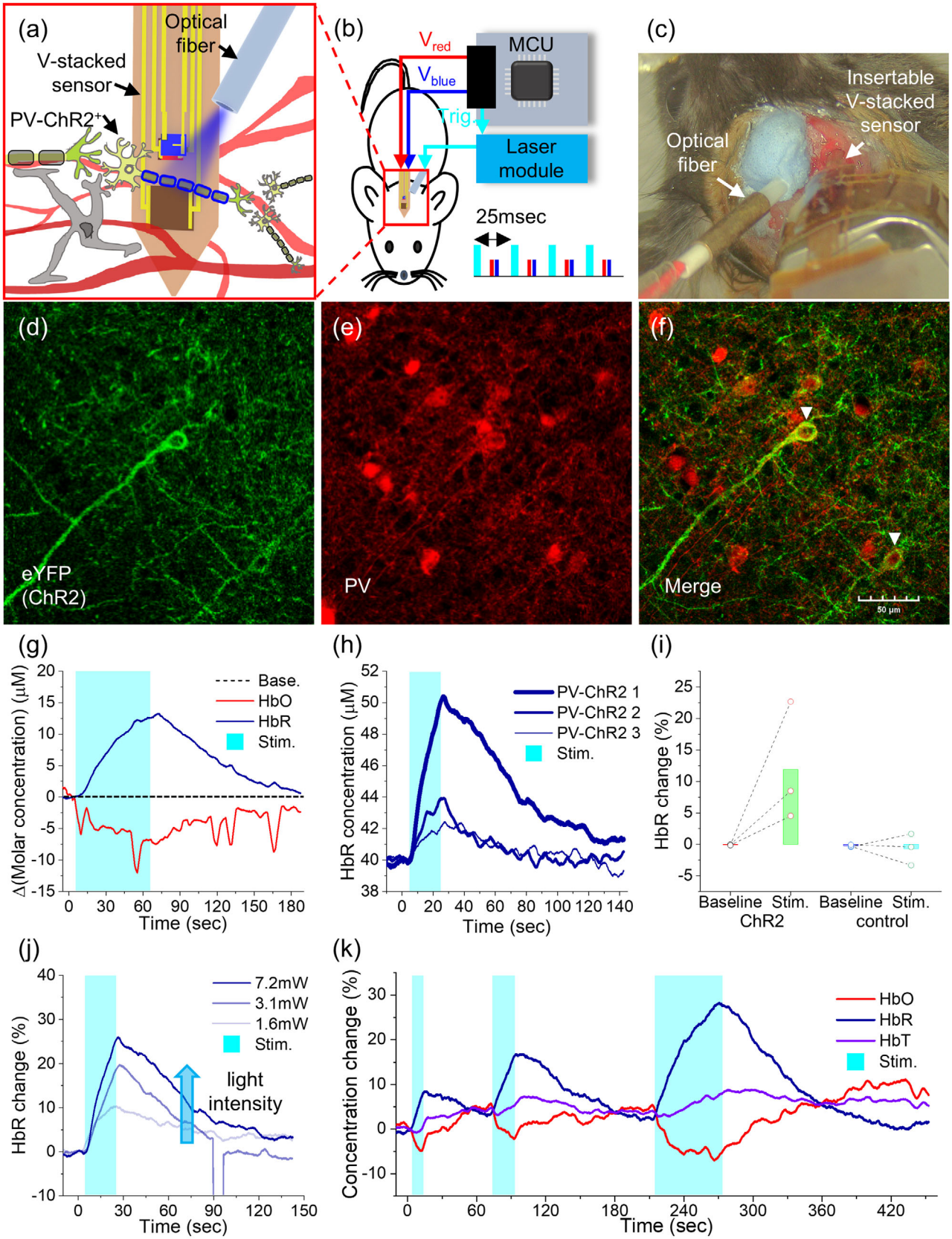

the sensor insertion depth and the distance to the target region, to avoid extremely low optical signal intensity with a longer interoptode distance. More details described in Figures S9 and S10 (Supporting Information).

Figure 5b shows a customized experimental setup to control optical stimulation from the laser module and hemodynamics monitoring from the V-stacked sensor, in a single programmable MCU for time scheduling (alternative switching, periods, intervals, recording etc). The stimulation by the laser module is driven at a 40 Hz frequency (period: 25 msec) with a 20% duty ratio (pulse width: 5 msec) to induce gamma band oscillations which consume oxygen (Detailed mechanisms are in Supporting Information), while measuring with the V-stacked sensor by alternatively turning on the red and blue LEDs for 5 msec during the laser off-state to avoid optical interference. The blue LED in the sensor does not activate ChR2 because of the low intensity (0.15–0.20 mW mm^{-2}).[23] More details are in Figure S13 (Supporting Information). The optical image after the surgery is in Figure 5c. The immunostaining fluorescence images of eYFP-tagged ChR2 (green) and the parvalbumin neurons (red) are in Figure 5d,e, respectively. The merged image in Figure 5f clearly indicates that ChR2 is expressed in the PV neurons as marked by white triangles.

The measurement result of concentration changes of oxyhemoglobin (HbO, red line) and deoxyhemoglobin (HbR, navy line) are shown in Figure 5g. As soon as the optogenetic stimulation (3.1 mW) is given at 5 s and maintained for 60 s (cyan box), immediate change in localized HbO and HbR concentrations occur while stimulating PV neurons.[13,14] This is because oxygen is required due to gamma band oscillation, which is a neural network activity induced by optogenetic stimulation of PV neurons.[24–26] More detailed description is in the supporting information. In separate experiments with optical stimulation (20 s, 40 Hz, 7.2 mW, pulse width: 5 msec) in PV-ChR2 mice ($n = 3$), the hemodynamic responses are observed as in Figure 5h. For all the animal models, consistent responses, increasing in HbR concentration is observed.[13,17] The experimental results are summarized to compare with a control group in Figure 5i. The averaged changes in HbR concentration for 5 s before stimulation (Baseline) and for 5 s before the end of stimulation (Stim.) are plotted for both of the ChR2 group (PV-ChR2-eYFP, $n = 3$) and control group (PV-GFP, $n = 3$), showing consistent increase in HbR concentration in the ChR2 group in contrast to the control group. The differences in the HbR concentration change observed in the ChR2 group across the animal models appear to be due to varying levels of ChR2 expression in each individual, as shown in Figure S14 (Supporting Information).

Although the experimental results indicate that HbR concentration changes by optogenetic stimulation can be clearly detected, it should be also noted that the number of animals per group ($n = 3$) is not enough to indicate statistical significance as statistical analysis using the two-tailed non-parametric Mann–Whitney U test, yielded a p-value of 0.81. Given the limited availability of transgenic mice, the experiments were conducted on three animals per group (experimental: PV-ChR2-eYFP, control: PV-GFP) to assess neurovascular hemodynamic changes induced by ChR2-mediated activation of parvalbumin neurons on the same Cre-positive mouse line in order to minimize potential variability arising from genetic background, Cre expression, and viral delivery. We acknowledge that a larger sample size would be necessary to achieve robust statistical validation.

The V-stacked hemodynamic sensor can detect localized HbR changes depending on stimulation intensity as shown in Figure 5j. With higher stimulating intensity (1.6 mW→ 3.1 mW → 7.2 mW), more steep increases of HbR change are observed with the V-stacked sensor. The measurements with repetitive stimulation in different durations (3.1 mW, 10, 20, 60 s in Figure 5k) clearly indicate that the V-stacked sensor can monitor optogenetically-induced localized neurovascular hemodynamic activities.

3. Conclusion

The results reported here confirm that hemodynamics monitoring is achievable with the vertically-stacked multicolor μLEDs and a photodetector integrated in a compact form onto a thin film substrate as demonstrated with a human subject and animal models. The benefits of the vertically stacking design come from maximized common paths in the tissues with the reduced active sensor size, enabling localized neuronal hemodynamics monitoring, which is crucial for interpreting and understanding brain functions. The localized monitoring capability of the V-stacked hemodynamic sensor can be further improved by implementing additional functionalities, such as neuronal action potential recording with a microelectrode array (MEA), thereby enabling deeper understating about the correlation between neuronal activity and neurovascular hemodynamics, which is known as neurovascular coupling (NVC). Unlike the conventional hemodynamics monitoring systems, this compactness and

Figure 5. Optogenetically-induced localized neurovascular hemodynamics monitoring. a) Schematic illustration of the inserted V-stacked sensor to monitor hemodynamics optically-stimulated by an optical fiber to the parvalbumin neurons expressing channelrhodopsin-2 (ChR2) through adeno-associated virus (AAV) injection. b) Experimental setup. All the time schedules (starting points, intervals, periods) of optogenetic stimulation by the laser module and measurement by the hemodynamic sensor are controlled by one programmable MCU. The photocurrents from the sensor are also recorded in the MCU. c) Optical microscope image of the mouse model to monitor neurovascular hemodynamics. d–f) Immunostained fluorescence images of (d) the ChR2, (e) parvalbumin neuron, and (f) merged one in the somatosensory barrel field region of a mouse. The white marks indicate the parvalbumin neurons expressing ChR2. g) Measurement results of neurovascular dynamics following the optical stimulation (cyan box) of the PV-ChR2 in the mouse barrel field region. Neuronal activity causes oxygen consumption, leading to reduced oxyhemoglobin (HbO, red line) and increased deoxyhemoglobin (HbR, navy line) concentration compared to the baseline (Base., black dashed line). h) Molar concentrations of HbR induced by optical stimulation (20 s, 40 Hz, 7.2mW, pulse width: 5 msec) (PV-ChR2-eYFP, $n = 3$). i) HbR concentration changes by the same optical stimulation (20 s, 40 Hz, 7.2 mW, pulse width: 5 msec) for the group with ChR2 (PV-ChR2-eYFP, $n = 3$) and the control group (PV-GFP, $n = 3$). GFP: green fluorescence protein, eYFP: enhanced yellow fluorescence protein. Baseline: average HbR for 5 s before stimulation, Stim.: average HbR for 5 s before stopping stimulation. j) HbR concentration changes depending on the stimulating optical power (1.6 to 7.2 mW). k) Measurements of optogenetically-induced neurovascular hemodynamics by repetitive stimulation with different stimulating durations (10, 20, 60 s).

extensibility of the V-stacked sensor could lead to useful tools for diverse brain research.

4. Experimental Section

Preparation of the GaAs Photodetector and AlGaInP Red LED on Each GaAs Wafer: The GaAs photodetector and AlGaInP red LED were prepared on each GaAs wafer with an epitaxially grown process and then, fabricated by several steps of photolithography and wet etching process, as reported previously.[2,27] Thin metal contact electrode (Ti/Au: 20 nm/80 nm, electron beam evaporation) was formed on the top contact layer (n-GaAs of photodetector and *p*-GaAs of red LED) by lift-off process with negative photoresist (AZ nLOF 2070, 7 µm, MicroChemicals), followed by the wet etching process with citric acid ($C_6H_8O_7$, monohydrate, J.T. Baker Inc.) and hydrogen peroxide (H_2O_2, 35%, OCI Company Ltd.) solution to define GaAs top contact layer. Each active device area (photodetector: 500 × 500 µm^2, red LED: 250 × 250 µm^2) was protected by photoresist (AZ 5214-E, 1.8 µm, AZ Electronics Materials). Then, the GaAs photodetector was fully etched down to the bottom contact layer with phosphoric acid (H_3PO_4, 85%, OCI Company Ltd.) and hydrogen peroxide solution to fabricate a vertical structure.[28] The AlGaInP red LED active area was sequentially etched with phosphoric acid solution and hydrochloric acid (HCl, 35%, OCI Company Ltd.) until the bottom contact layer (n-GaAs). Slightly large area (250 × 300 µm^2) contained with the active and the bottom contact region was protected with photoresist (AZ5214-E), followed by wet etching to remove the remain bottom contact layer. The bottom contact metal (Ti/Au: 20 nm/80 nm, electron beam evaporation) was formed by lift-off process. The defined red LEDs were protected with thin polymer (SU-8 2002, 2 µm, Kayaku Advanced Materials) to prevent unwanted damage. Both photodetector and red LED defined devices were covered with thick photoresist (AZ 10XT, 10 µm, Merck) to protect them from chemical and mechanical damages during the subsequent process.

Preparation of the GaN Blue LED on a Si Wafer: The GaN blue LED layers epitaxially grown on the Si substrate were dry-etched by inductively coupled plasma reactive ion etching (ICP-RIE, Oxford Instruments), as reported previously.[29] The protective photoresist layer (AZ 10XT, 10 µm) covered all areas except the bottom contact areas (80 × 80 µm^2) during the ICP-RIE mesa etching process (BCl_3, Cl_2, RF power: 50 W, ICP power: 300 W). Also, the patterned nickel (800 nm, DC sputtering) formed with blue LED size (250 × 300 µm^2) by lift-off process was used as a etch mask during LED device isolation through second ICP-RIE process (BCl_3, Cl_2, Ar, RF power: 125 W, ICP power: 500 W). During this second ICP-RIE process, Si substrate was also etched ≈2 µm deeper than the isolated blue LED devices for under-cut process. Sequential lift-off processes were conducted to fabricate the thin metal spreader (Ni/Au: 5 nm/5 nm) and the contact metal (Ni/Au: 20 nm/100 nm), followed by annealing on a hotplate at 300 °C for 1 h to enhance the adhesion between the GaN and the deposited metal. To separate the blue LED devices from the Si wafer, immersed in a potassium hydroxide (KOH, 45%, Samchun Chemicals) double boiled solution on a hotplate at 110 °C, allowing for anisotropic etching of silicon perpendicular to the <110> plane until the width of the silicon pillars under the blue LED devices reached ≈10 µm. It could be confirmed under the optical microscope because the light in the visible wavelength range was nearly transmitted through the GaN layer.

Migration the GaN Blue LEDs on a Bare Si Wafer: The fabricated GaN blue LEDs on the silicon wafer, were migrated to a new bare silicon wafer for further processing. A glass substrate coated with polymethyl methacrylate (PMMA, 2 µm, Kayaku Advanced Materials) was prepared as a temporary handling substrate, followed by coating with photoresist (SU-8 2002, 1000 rpm., 10 s) acting as an adhesive. The Blue LEDs on the silicon wafer were then inverted and bonded onto the SU-8 layer. A 50 g weight was placed on the backside of the inverted silicon wafer, and after waiting more than 5 h, UV light was exposed (300 mJ cm^{-2}), followed by baking at 110 °C for 20 min to fully cure the adhesive. Then, immersing the handling substrate attached with blue LEDs on the silicon wafer in the KOH double boiled solution on a hotplate at 150 °C solution for 20 min to dissolve the remaining silicon pillars. As a result, the silicon wafer detached, and the blue LEDs were migrated onto the temporal handling substrate. The temporary handling substrate was immersed in DI water to carefully detach the glass and the polymer film with the inverted blue LEDs. The film was flipped and placed onto a new bare silicon wafer. Finally, dry-etching the polymer layer (PMMA: 2 µm, SU-8: 4 µm) covered the blue LEDs by using the polymer RIE (O_2: 100 mTorr, RF power: 100 W), enables the transfer-printing of the blue LEDs with a sticky elastomeric stamp (PDMS, polydimethylsiloxane).

Integration of the GaAs Photodetector and AlGaInP Red LED Onto the PI Film Substrate: Each photodetector and red LED, covered with protective photoresist, was attached to a PI film stamp coated with a PDMS layer, respectively, and immersed in hydrochloric acid solution heated on a hotplate at 40 °C for 40 min. After dissolving the sacrificial layer, the photodetector and red LED were released from each GaAs wafer while attached to the film stamp. First, to integrate the photodetector onto the target PI film substrate (25 µm), the metal (Ni/Au: 20 nm/100 nm, electron beam evaporation) was deposited on the bottom surface of the photodetector with film stamp and on the PI substrate as a bottom electrode. The two metal-coated surfaces were placed directly in contact, followed by applying heat (95 °C) and pressure (2.5 Mpa) for 5 min resulting in a direct metal-to-metal bonding between the photodetector and the PI substrate. Then the film stamp was carefully peeled off. To remove any PDMS residue that may have transferred from the film stamp to the PI substrate, immersed in hydrofluoric acid (HF, 50%, Duksan Pure Chemicals) for 30 s and cleaned. The bottom electrode of photodetector was defined by photoresist (AZ 5214-E) and then wet etched with respective metal etchant (Ni, Au). The photodetector device were encapsulated with epoxy insulation layer (SU-8 2002), except for top and bottom electrodes, and formed metal (Cr/Au: 100 nm/250 nm) interconnection by lifting-off process. Additionally, encapsulated with SU-8 was performed again, remaining the pads for electrical connection by photolithography process.

After completing the fabrication process for the photodetector, a thin layer of epoxy, as an interlayer adhesive was applied by spin coating (SU-8 2000.5, 1000 rpm., 5 s). The red LED, attached to its film stamp was aligned, next to the photodetector and then put a elastomeric block (PDMS) and a 100 g weight on the film stamp for more than 6 h. UV light was exposed (300 mJ cm^{-2}), followed by baking at 110 °C for 20 min to fully cure the interlayer adhesive. After carefully removed the film stamp of red LED, encapsulations and interconnections for the red LED were formed through lithography processes, following the same procedure used for the photodetector. More details about fabrication process are described in Figure S15 (Supporting Information).

Integration of the GaN Blue LED Onto the PI Film Substrate: The blue LEDs migrated on the bare silicon wafer, was selectively detached using a protruded sticky PDMS stamp (25:1) fabricated by a molding process (mold: patterned SU-8 2075 on silicon wafer). More details are described in Figure S16 (Supporting Information). An interlayer adhesive was also spin-coated (SU-8 2000.5, 1000 rpm., 5 s) on the PI film substrate, on which photodetector and red LED devices were integrated. The blue LED was aligned directly above the location of the red LED integrated on the PI substrate, and then exposed UV light (300 mJ cm^{-2}) and baked at 110 °C for 20 min to fully cure the interlayer adhesive layer. After carefully remove the protruded PDMS stamp, encapsulations and interconnections for the blue LED was formed by following the above procedure. Stacking LEDs also can be done in different ways as reported for other applications including displays[30,31] and stimulations.[32,33]

Preparation of the V-Stacked Hemodynamic Sensor for Human Subject and Animal Model: For the sensor device isolation, all regions except for the components that make up the sensor, such as the electrodes, photodetectors and LEDs, were removed using polymer RIE (RIE mask: Ti 50 nm). To fabricate a flexible sensor that can be attached to the human subject body, the whole surfaces of the isolated device were coated with a sticky silicone elastomer (PDMS, 30:1). In the case of the implantable V-stacked hemodynamic sensor for animal model, the isolated device required a moisture barrier to protect it in the humid environment of the body.[34] The isolated device was encapsulated with SU-8 and PDMS using a dip-coating method, and a biocompatible polymer, parylene C (10 µm), was deposited by chemical vapor deposition.

Measurement of Electrical and Optical Properties of Photodetector and LEDs: The current–voltage characteristics of photodetectors (GaAs) and LEDs (AlGaInP red LED and GaN blue LED) were measured by a source/measure unit (B2902A, Keysight Technologies). The electrical properties of photodetector were measured and compared under/ one sun illumination (AM1.5G) of a 3A solar simulator (XES-70S1, SAN-EI Electric Ltd.) before and after, repetitive bending or immersion in PBS solution. External quantum efficiency (EQE) of photodetector was measured in the wavelength range from 325 to 1100 nm using a quantum efficiency measurement system (QuantX-300, Newport). The characteristics of red and blue LEDs were measured by pulsed sweep mode (on time: 10 milliseconds, off time: 100 milliseconds) to prevent temperature change caused by previous pulsed operation of each LED. Also, the emission spectra of vertically stacked LEDs were measured with an optical spectrometer (avaspec-ULS2048L, Avantes Corp.). The measurements were conducted both when each LED was operated independently and when two LEDs were operated simultaneously.

Preparation for Measuring Heart Rate and Oxygen Saturation Change in Human Subject: The V-stacked hemodynamic sensor was firmly attached to the index finger of a subject with the aid of tape to prevent unwanted light path due to air gap between the sensor and skin. Commercial ECG pads (EVAL-AD8233, Analog Devices) for measuring heart rate was placed on the chest to compare the period between PPG signal, and a commercial pulse oximeter (bedside SpO_2 monitoring system, Nellcor) probe for oxygen saturation comparison was attached to the middle finger. Two breathing bags (60 L each) were manually filled with different composition (Bag 1: O_2 21%/N_2 79%, Bag 2: O_2 10%/N_2 90%) of medical oxygen and nitrogen, while monitoring gas flow meter and allowed to diffuse for over 1 h before the experiment. The gas composition ratio of these bags was measured by oxygen concentration sensor. The subject wore a face mask that enabled breathing only with the gas bag, and the non-rebreathing valve attached to the mask prevented the exhaled air from re-entering the gas bag, allowing the subject to continuously inhale air with the constant oxygen concentration. The gas bag used for breathing could be switched through a three-way valve connected to the two gas bags and the face mask. The human subject experiments for measuring heart rate and oxygen saturation were conducted with informed consent obtained from all participants and approved by the institutional review board (IRB) at Gwangju Institute of Science and Technology (20230202-HR-70-05-02).

Optical Analysis of V-Stacked Sensor on Skin: Optical simulations (Ansys Zemax OpticStudio) were performed to visualize the photon paths detected by the photodetector, where photons from the red (670 nm) and blue (460 nm) light emitted by the LEDs were scattered and absorbed by the skin tissue, using the Henyey–Greenstein bulk scatter model.[35,36] The optical properties used in the simulation and calculation were as follows: for oxyhemoglobin, the molar extinction coefficient (ε_a) was set to 44480 $cm^{-1}M^{-1}$ at 460 nm and 294 $cm^{-1}M^{-1}$ at 670 nm, for deoxyhemoglobin, the molar extinction coefficient (ε_a) was set to 23389 $cm^{-1}M^{-1}$ at 460 nm and 2795 $cm^{-1}M^{-1}$ at 670 nm, for brain, the absorption coefficient (μ_a) was set to 0.6 mm^{-1} at 460 nm and 0.04 mm^{-1} at 670 nm; the scattering coefficient (μs) was set to 23.7 mm^{-1} at 460 nm and 15.1 mm^{-1} at 670 nm,[37] and for human skin, the absorption coefficient (μ_a) was set to 0.9 mm^{-1} at 460 nm and 0.08 mm^{-1} at 670 nm; the scattering coefficient (μs) was set to 67 mm^{-1} at 460 nm and 26 mm^{-1} at 670 nm, and the anisotropic scattering factor (g) was set to be 0.9.[21,38] For visual clarity, only the photon paths from the LEDs that enter the photodetector were depicted. To count the number of tissue voxels traversed by photons based on the LED arrangements, the optical simulation results were exported and programmed using simple Python code. The size of each voxel was set to $10 \times 10 \times 10$ μm^3 and 2.5×10^5 rays were simulated for each color.

Animal Experiments 1. Heart Rate and Oxygen Saturation Change: In vivo experiments for measuring heart rate by PPG and oxygen saturation change by using V-stacked hemodynamic sensor were conducted with hairless mice (SKH1-Hr^{hr}, 12–16 weeks old, ≈30 g). The surgical procedures and experiments using animal models were conducted following the methods described in the previous research.[27,39,40] The mice were initially anesthetized via intraperitoneal injection of a mixture containing ketamine (50 mg kg^{-1}, Yuhan Ketamine 50, Yuhan), xylazine (5 mg kg^{-1}, Rompun Inj., Bayer Corp.,) and saline solution (Normal Saline Inj., Dae Han Pharm Co. Ltd.) with a total volume of 0.3 mL. After confirming effective anesthesia through tail pinch test, a small incision (≈3 mm) was made around the visible femoral vessel to insert the V-stacked hemodynamic sensor. For hypoxic challenge test, the mice were placed in a custom-made acrylic chamber, where the oxygen concentration was modulated manually by adjusting the flow rate of supplied gas (medical O_2 and N_2). The oxygen concentration sensor probe was placed near the facial region to measure the oxygen concentration of the inhaled gas. The animal experiments were conducted with approval from the Institutional Animal Care and Use Committee (IACUC) of Gwangju Institute of Science and Technology (GIST-2024-038).

Animal Experiments 2. Neurovascular Hemodynamics by Optogenetic Stimulation—Animals: Experiments were conducted using adult male parvalbumin (PV)-Cre transgenic mice (3-4 months old, The Jackson Laboratory, Stock No. 008069). Mice were maintained under controlled environmental conditions with standard 12 h light-dark cycles (lights on at 07:00, off at 19:00) at 22 ± 2 °C and 50 ±10% relative humidity. Animals had free access to food and water ad libitum throughout the experimental period. Mice were group-housed (4-5 per cage) in standard laboratory cages until viral injection surgery, after which they were individually housed until used for experiments. All experimental procedures were conducted in accordance with protocols approved by the Institutional Animal Care and Use Committee (IACUC) of Gwangju Institute of Science and Technology (GIST-2024-052).

Animal Experiments 2. Neurovascular Hemodynamics by Optogenetic Stimulation—Virus Injections: For stereotaxic injection, mice were anesthetized with isoflurane (1–3%) delivered in oxygen (0.8–1 L min^{-1}) and positioned in a stereotaxic apparatus (Model 51615, Stoelting Co., Wood Dale, IL, USA). An analgesic, ketoprofen (5 mg kg^{-1}, subcutaneously), was administered prior to surgery. The surgical area was shaved, cleaned with 70% ethanol and povidone-iodine, and a midline scalp incision was made to expose the skull. To achieve targeted expression, a viral vector was unilaterally injected into the primary somatosensory barrel field (S1BF) using stereotaxic coordinates relative to bregma: anterior-posterior (AP): −0.9 mm; medial-lateral (ML): +3 mm; dorsal-ventral (DV): −1.5 mm. The experimental group received AAV5-EF1α-DIO-hChR2(H134R)-EYFP-WPRE-pA to express channelrhodopsin-2 (ChR2) in Cre-expressing neurons, while the control group received AAV-DJ-EF1α-DIO-GFP to express GFP. Each virus was administered to its respective group at a volume of 1 μL, infused at a rate of 0.1 μL min^{-1}. The injection needle remained in place for an additional 10 min to prevent backflow. Following suture of the scalp incision, mice were placed on a heating pad for post-surgical recovery. For post-operative pain management, ketoprofen was additionally administered on the day following surgery. All experimental procedures were performed 4–6 weeks post-injection to ensure sufficient recovery and Cre-mediated recombination.

Animal Experiments 2. Neurovascular Hemodynamics by Optogenetic Stimulation—Stereotaxic Surgery: Four to six weeks after viral injection, a surgical procedure was performed to implant an optical fiber and a V-stacked sensor, targeting the site of viral injection. The optical fiber (200 μm core, NA = 0.39, Cat. No. FT200EMT, Thorlabs, Newton, NJ, USA) coupled to a ferule (1.25 mm, Cat. No. CFLC230-10, Thorlabs, Newton, NJ, USA) was implanted 300 μm distal to the virus injection site at a 30-degree angle to minimized interference with the subsequently inserted V-stacked sensor and secured to the skull and anchor screw with dental acrylic (Cat. No. 0921375, Bosworth Fastray; Keystone Ind, Gibbstown, NJ, USA). The V-stacked sensor was then inserted 300 μm posterior to the virus injection site, ensuring its LED and photodetector precisely targeted the injected region. Stimulation and recording were initiated at least 30 min after the implantation of both the optical fiber and V-stacked sensor.

Supporting Information

Supporting Information is available from the Wiley Online Library or from the author.

Acknowledgements

T.L. and J.J. contributed equally to this work. This work was supported by the National Research Foundation of Korea (NRF) grant funded by the Korea Government (Ministry of Science and ICT, MIST and Ministry of Health and Welfare; No. RS-2023-00277831 to J.L. and No. HU22C0150 to T.K.), the Samsung Research Funding & Incubation Center for Future Technology of Samsung Electronics (SRFC-IT1901-16 to J.L.), and the GIST-MIT Research Collaboration grant funded by the GIST.

Conflict of Interest

The authors declare no conflict of interest.

Data Availability Statement

The data that support the findings of this study are available in the supplementary material of this article.

Keywords

hemodynamics monitoring, heterogeneous integration, micro light emitting diode, optoelectronic sensor, optogenetics

Received: February 19, 2025
Revised: April 17, 2025
Published online:

[1] T. R. Ray, J. Choi, A. J. Bandodkar, S. Krishnan, P. Gutruf, L. Tian, R. Ghaffari, J. A. Rogers, *J. Am. Chem. Soc.* **2019**, *119*, 5461.
[2] J. Kim, N. Kim, M. Kwon, J. Lee, *ACS Appl. Mater. Interfaces* **2017**, *9*, 25700.
[3] J. Kim, G. A. Salvatore, H. Araki, A. M. Chiarelli, Z. Xie, A. Banks, X. Sheng, Y. Liu, J. W. Lee, K.-I. Jang, S. Y. Heo, K. Cho, H. Luo, B. Zimmerman, J. Kim, L. Yan, X. Feng, S. Xu, M. Fabiani, G. Gratton, Y. Huang, U. Paik, J. A. Rogers, *Sci. Adv.* **2016**, *2*, 1600418.
[4] A. Y. Rwei, W. Lu, C. Wu, K. Human, E. Suen, D. Franklin, M. Fabiani, G. Gratton, Z. Xie, Y. Deng, S. S. Kwak, L. Li, C. Gu, A. Liu, C. M. Rand, T. M. Stewart, Y. Huang, D. E. Weese-Mayer, J. A. Rogers, *Proc. Natl. Acad. Sci. USA* **2020**, *117*, 31674.
[5] C. Wu, A. Y. Rwei, J. Y. Lee, W. Ouyang, L. Jacobson, H. Shen, H. Luan, Y. Xu, J. Bin Park, S. S. Kwak, X. Ni, W. Bai, D. Franklin, S. Li, Y. Liu, X. Ni, A. M. Westman, M. R. Macewan, J. A. Rogers, M. A. Pet, *J Reconstr Microsurg* **2022**, *38*, 096.
[6] C. M. Lochner, Y. Khan, A. Pierre, A. C. Arias, *Nat. Commun.* **2014**, *5*, 5745.
[7] T. Yokota, P. Zalar, M. Kaltenbrunner, H. Jinno, N. Matsuhisa, H. Kitanosako, Y. Tachibana, W. Yukita, M. Koizumi, T. Someya, *Sci. Adv.* **2016**, *2*, 1501856.
[8] J. Kim, P. Gutruf, A. M. Chiarelli, S. Y. Heo, K. Cho, Z. Xie, A. Banks, S. Han, K. I. Jang, J. W. Lee, K. T. Lee, X. Feng, Y. Huang, M. Fabiani, G. Gratton, U. Paik, J. A. Rogers, *Adv. Funct. Mater.* **2017**, *27*, 1604373.
[9] M. H. Kang, G. J. Lee, J. H. Lee, M. S. Kim, Z. Yan, J. W. Jeong, K. I. Jang, Y. M. Song, *Adv. Sci.* **2021**, *8*, 2170057.
[10] W. Lu, W. Bai, H. Zhang, C. Xu, A. M. Chiarelli, A. Vázquez-Guardado, Z. Xie, H. Shen, K. Nandoliya, H. Zhao, K. Lee, Y. Wu, D. Franklin, R. Avila, S. Xu, A. Rwei, M. Han, K. Kwon, Y. Deng, X. Yu, E. B. Thorp, X. Feng, Y. Huang, J. Forbess, Z.-D. Ge, J. A. Rogers, *Sci. Adv.* **2021**, *7*, abe0579.
[11] H. Guo, W. Bai, W. Ouyang, Y. Liu, C. Wu, Y. Xu, Y. Weng, H. Zang, Y. Liu, L. Jacobson, Z. Hu, Y. Wang, H. M. Arafa, Q. Yang, D. Lu, S. Li, L. Zhang, X. Xiao, A. Vázquez-Guardado, J. Ciatti, E. Dempsey, N. Ghoreishi-Haack, E. A. Waters, C. R. Haney, A. M. Westman, M. R. MacEwan, M. A. Pet, J. A. Rogers, *Nat. Commun.* **2022**, *13*, 3009.
[12] H. Zhang, P. Gutruf, K. Meacham, M. C. Montana, X. Zhao, A. M. Chiarelli, A. Vázquez-Guardado, A. Norris, L. Lu, Q. Guo, C. Xu, Y. Wu, H. Zhao, X. Ning, W. Bai, I. Kandela, C. R. Haney, D. Chanda, R. W. Gereau, J. A. Rogers, *Sci. Adv.* **2019**, *5*, aaw0873.
[13] T. T. Vo, G. H. Im, K. Han, M. Suh, P. J. Drew, S.-G. Kim, *Proc. Natl. Acad. Sci. USA* **2023**, *120*, 2220777120.
[14] J. Lee, C. L. Stile, A. R. Bice, Z. P. Rosenthal, P. Yan, A. Z. Snyder, J. M. Lee, A. Q. Bauer, *J. Cereb. Blood Flow Metab.* **2021**, *41*, 841.
[15] K. Masamoto, T. Omura, N. Takizawa, H. Kobayashi, T. Katura, A. Maki, H. Kawaguchi, K. Tanishita, *J. Cereb. Blood Flow Metab.* **2003**, *23*, 1075.
[16] Y. Abe, S. Kwon, M. Oishi, M. Unekawa, N. Takata, F. Seki, R. Koyama, M. Abe, K. Sakimura, K. Masamoto, Y. Tomita, H. Okano, H. Mushiake, K. F. Tanaka, *Cell Rep.* **2021**, *36*, 109427.
[17] N. Offenhauser, K. Thomsen, K. Caesar, M. Lauritzen, *J. Physiology* **2005**, *565*, 279.
[18] M. Kim, J. Hong, J. Kim, H. Shin, *Biomed. Opt. Express* **2017**, *8*, 2781.
[19] M. Kim, J. Hong, H. Shin, *Biomed. Opt. Express* **2018**, *9*, 2699.
[20] S. W. Cramer, R. E. Carter, J. D. Aronson, S. B. Kodandaramaiah, T. J. Ebner, C. C. Chen, *J. Neurosci. Methods* **2021**, *354*, 109100.
[21] A. Kallepalli, J. Halls, D. B. James, M. A. Richardson, *J Biophotonics* **2022**, *15*, 202100275.
[22] International Organization for Standardization (ISO), ISO80601-2-61:2017. Medical electrical equipment-Part 2-61, *International Organization for Standardization*, Geneva, Switzerland, **2017**.
[23] A. Dawydow, R. Gueta, D. Ljaschenko, S. Ullrich, M. Hermann, N. Ehmann, S. Gao, A. Fiala, T. Langenhan, G. Nagel, R. J. Kittel, *Proc. Natl. Acad. Sci. USA* **2014**, *111*, 13972.
[24] O. Kann, C. Huchzermeyer, R. Kovács, S. Wirtz, M. Schuelke, *Brain* **2011**, *134*, 345.
[25] F. Du, X.-H. Zhu, Y. Zhang, M. Friedman, N. Zhang, K. Uğurbil, W. Chen, *Proc. Natl. Acad. Sci. USA* **2008**, *105*, 6409.
[26] O. Kann, I. E. Papageorgiou, A. Draguhn, *Nature Publishing Group* **2014**, *34*, 1270.
[27] J. Kim, J. Seo, D. Jung, T. Lee, H. Ju, J. Han, N. Kim, J. Jeong, S. Cho, J. H. Seol, J. Lee, *Proc. Natl. Acad. Sci. USA* **2020**, *117*, 16856.
[28] J. Kim, J. Hwang, K. Song, N. Kim, J. C. Shin, J. Lee, *Appl. Phys. Lett.* **2016**, *108*, 253101.
[29] H. Kim, E. Brueckner, J. Song, Y. Li, S. Kim, C. Lu, J. Sulkin, K. Choquette, Y. Huang, R. G. Nuzzo, J. A. Rogers, *Proc. Natl. Acad. Sci. USA* **2011**, *108*, 10072.
[30] L. Li, G. Tang, Z. Shi, H. Ding, C. Liu, D. Cheng, Q. Zhang, L. Yin, Z. Yao, L. Duan, D. Zhang, C. Wang, M. Feng, Q. Sun, Q. Wang, Y. Han, L. Wang, Y. Luo, X. Sheng, *Proc. Natl. Acad. Sci. USA* **2021**, *118*, 2023436118.
[31] J. Shin, H. Kim, S. Sundaram, J. Jeong, B. I. Park, C. S. Chang, J. Choi, T. Kim, M. Saravanapavanantham, K. Lu, S. Kim, J. M. Suh, K. S. Kim, M. K. Song, Y. Liu, K. Qiao, J. H. Kim, Y. Kim, J. H. Kang, J. Kim, D. Lee, J. Lee, J. S. Kim, H. E. Lee, H. Yeon, H. S. Kum, S. H. Bae, V. Bulovic, K. J. Yu, K. Lee, et al., *Nature* **2023**, *614*, 81.
[32] L. Li, L. Lu, Y. Ren, G. Tang, Y. Zhao, X. Cai, Z. Shi, H. Ding, C. Liu, D. Cheng, Y. Xie, H. Wang, X. Fu, L. Yin, M. Luo, X. Sheng, *Nat. Commun.* **2022**, *13*, 839.
[33] D. Mao, F. Sun, B. Driscoll, Z. Li, G. Xu, *Cell Rep Phys Sci* **2023**, *4*, 101702.
[34] J. Park, K. Kim, Y. Kim, T. S. Kim, I. S. Min, B. Li, Y. U. Cho, C. Lee, J. Y. Lee, Y. Gao, K. Kang, D. H. Kim, W. J. Choi, H.-B. Shin, H. K.

Kang, Y. M. Song, H. Cheng, I.-J. Cho, K. J. Yu, *Sci. Adv.* **2023**, *9*, adi8918.
[35] L.-G. Henyey, J.-L. Greenstein, *Astrophys. J.* **1941**, *93*, 70.
[36] S. Leyre, F. B. Leloup, J. Audenaert, G. Durinck, J. Hofkens, G. Deconinck, P. Hanselaer, *Appl. Opt.* **2013**, *52*, 4083.
[37] S. L. Jacques, *Phys. Med. Biol.* **2013**, *58*, R37.
[38] A. N. Bashkatov, E. A. Genina, V. I. Kochubey, V. V. Tuchin, *J Phys D Appl Phys* **2005**, *38*, 2543.
[39] D. Jung, K. Song, H. Ju, H. Park, J. H. Han, N. Kim, J. Kim, J. Lee, *Adv. Healthcare Mater.* **2021**, *10*, 2001480.
[40] D. Jung, H. Ju, S. Cho, T. Lee, C. Hong, J. Lee, *npj Flexible Electron.* **2024**, *8*, 13.